# Synthesis, Characterization, and Catalytic Performances of Novel CoMo Hydrodesulfurization Catalysts Supported on Mesoporous Aluminas

Nela Bejenaru,[†] Christine Lancelot,[†] Pascal Blanchard,[†] Carole Lamonier,[†] Loïc Rouleau,[‡] Edmond Payen,[†] Franck Dumeignil,*[,†] and Sébastien Royer*[,§]

*UCCS, UMR CNRS 8181, Université des Sciences et Technologies de Lille, Bât. C3, 59655 Villeneuve d'Ascq Cedex, France, LACCO, UMR CNRS 6503, Université de Poitiers, F-86022 Poitiers Cedex, France, Département Catalyse et Séparation, IFP-Lyon, BP3, 69390 Vernaison, France*

*Received July 30, 2008. Revised Manuscript Received December 6, 2008*

A series of mesoporous aluminas of different morphologies was prepared using synthesis methods recently described in the literature. These aluminas were used as supports for CoMo HDS catalysts that were fully characterized. Their performances were evaluated using an atmospheric thiophene HDS catalytic test. The properties of the mesostructured alumina-based catalysts were compared with those of a conventional alumina-based CoMo catalyst and of a previously optimized sol−gel alumina-based catalyst (reference aluminas). The highest conversion was observed when using the alumina prepared from Al-sec-butoxide with P123 as a templating agent, which exhibited the largest mesopores and a fine fibrillar morphology, with a result ca. 25% larger than that observed on both reference aluminas. According to their catalytic behavior, the samples were divided into two groups, the first one comprising the low conversion catalysts, and the second one comprising the high conversion catalysts. Among all the considered parameters (physical properties of the solids, oxidic phase nature, sulfidic phase morphology), only the difference in the state of the oxo-molybdate phase gave a reliable correlation with catalytic performances. In the oxidic form, the low activity samples presented monomolybate species, whereas the high activity samples presented polymolybdate species.

## 1. Introduction

The sulfur-containing compounds present in transportation fuels are responsible for a substantial degradation extent of the air quality.[1] They are also strong poisons of the catalysts used in vehicles' exhaust gas converters.[2] To clear these issues, legal limitations on the sulfur content are more and more stringent. The maximum sulfur content in gas oil in the US has been decreased to 15 ppm in 2006.[3] Japan has already imposed a maximal sulfur concentration of 10 ppm since 2007[2] and the same regulation will take place in the EU by 2009.[4] To comply with the forthcoming regulations, enhancement of the efficiency of the hydrodesulfurization (HDS) processes is needed. Improvement of the catalytic formulations is the most straightforward solution.

The active phase of conventional HDS catalysts consist of well dispersed nanometric $MoS_2$ crystallites dispersed on a $\gamma$-$Al_2O_3$ support[5] and promoted with cobalt atoms (CoMoS phase) or nickel atoms (NiMoS phase). These promotor atoms that are located at the edges and corners of the disulfide slabs, are responsible for enhanced HDS catalytic performances.[6,7] The most convenient and thus widespread method for obtaining these active phases is the sulfidation of an oxidic precursor obtained by incipient wetness impregnation of a support with an ammonium heptamolybdate (AHM) based solution.[8−10] Note that more sophisticated methods such as impregnation of heteropolycompounds[11−14] and chemical vapor deposition (CVD)[15,16] generally lead to higher HDS

* To whom correspondence should be addressed. Tel.: 33-(0)3-20-43-45-38(F.D.); 33-(0)5-49-45-40-48(S.R.). Fax: 33-(0)3-20-43-65-61 (F.D.); 33-(0)5-49-45-33-4(S.R.). E-mail: franck.dumeignil@univ-lille1.fr(F.D.); sebastien.royer@univ-poitiers.fr.

[†] Université des Sciences et Technologies de Lille.

[‡] IFP-Lyon.

[§] Université de Poitiers.

(1) Babich, I. V.; Moulijn, J. A. *Fuel* **2003**, *82* (6), 607.

(2) Central Environment Council. *Future Policy for Motor Vehicles Exhaust Emission Reduction (7th report)*; Japanese Ministry of the Environment: Tokyo, 2003.

(3) Environmental Protection Agency. *Fed. Regist.* **2001**, *66* (12), 5101−5150.

(4) *Directive of the European Parliament and of the Council on the Quality of Petrol and Diesel Fuels*; European Parliament: Brussels, Belgium, 2001; p 241.

(5) Prins, R.; de Beer, V. H. J.; Samorjai, G. A. *Catal. Rev. Sci. Eng.* **1989**, *31*, 1.

(6) Topsoe, N. Y.; Topsoe, H. *J. Catal.* **1982**, *75*, 354.

(7) Candia, R.; Topsoe, N. Y.; Clausen, B. S.; Wivel, C.; Nevald, R.; Morup, S.; Topsoe, H. *Proceedings of the 4th International Conference on Chemistry and Uses of Molybdenum*, Golden, CO, Aug 9−13, 1982.

(8) Al-Zeghayer, Y. S.; Sunderland, P.; Al-Masry, W.; Al-Mubaddel, F.; Ibrahim, A. A.; Bhartiya, B. K.; Jibril, B. Y. *Appl. Catal., A* **2005**, *282*, 163.

(9) Dumeignil, F.; Sato, K.; Imamura, M.; Matsubayashi, N.; Payen, E.; Shimada, H. *Appl. Catal., A* **2005**, *287*, 135.

(10) Dumeignil, F.; Sato, K.; Imamura, M.; Matsubayashi, N.; Payen, E.; Shimada, H. *Appl. Catal., A* **2006**, *315*, 18.

(11) Damyanova, S.; Spozhakina, A.; Shopov, D. *Appl. Catal.* **1989**, *48*, 177.

(12) Maitra, A. M.; Cant, N. W.; Trimm, D. L. *Appl. Catal., A* **1989**, *48*, 187.

(13) Griboval, A.; Blanchard, P.; Payen, E.; Fournier, M.; Dubois, J. L. *Catal. Today* **1998**, *45*, 277.

(14) Martin, C.; Lamonier, C.; Fournier, M.; Mentré, O.; Harlé, V.; Guillaume, D.; Payen, E. *Chem. Mater.* **2005**, *17*, 4438.

(15) Okamoto, Y.; Ishihara, S. Y.; Kawano, M.; Satoh, M.; Kubota, T. *J. Catal.* **2003**, *217*, 12.

10.1021/cm802084e CCC: $40.75 
Published on Web 01/15/2009

activities. The HDS performances strongly depend on the nature of the support.[17−21] A large variety of "conventional" supports such as $SiO_2$,[22] $TiO_2$,[23−26] $ZrO_2$,[27−29] zeolites[30] and mixed oxides,[31−36] has already been used for HDS catalysts. The recent developments in the field of the synthesis of mesostructured oxides offer further perspectives for catalytic applications. Since the first reports on the synthesis of silica based mesoporous molecular sieves of the M41S family in 1992,[37,38] considerable efforts have been devoted to the development of new routes for optimizing the synthesis of pure or modified (by grafting or substitution) mesostructured $SiO_2$. Some reviews concerning the synthesis and the use in catalysis of this kind of materials can be found.[39−43] Since the middle of the 1990s, these new mesostructuration methodologies were adapted to enable the synthesis of other oxides like $Al_2O_3$,[44−46] $TiO_2$,[47−49] $ZrO_2$,[50−53] and $CeO_2$.[54] Mesostructured materials exhibit various advantages for catalytic applications such as a particularly high surface area with a pore size in the mesopore range, which can be easily tailored (typically between 2 and 15 nm). However, only the mesostructured silica-based materials, which were first discovered, were extensively studied as HDS catalysts supports; pure mesoporous silica was used by Sorensen et al.[55] and Sampieri et al.[56] The effect of the incorporation of Al atoms in the mesostructured silica network using different Si/Al ratios was also studied[57−60] Some elements like Ti,[61−64] Zr,[64] and Nb[65] were also grafted on the surface or incorporated into the walls of the silica before formation of the HDS active phase; Recently, Guttierez et al.[66] prepared NiMo catalysts using SBA-15 material covered with $ZrO_2$ monolayer as a support, with an important increase in the catalytic activity in deep HDS. In contrast, the literature concerning the use of nonsiliceous mesostructured oxides for HDS reactions is scarce. From our knowledge, only Hicks et al.[67] and Kaluza et al.[68] have reported the use of mesostructured alumina as a support for the HDS of dibenzothiophene and


(16) Lee, J. J.; Kim, H.; Koh, J. H.; Jo, A.; Moon, S. H. *Appl. Catal., B* **2005**, *58*, 89.
(17) Grimblot, J.; Bonnelle, J.-P. *J. Electron Spectrosc. Relat. Phenom.* **1976**, *9*, 449.
(18) Clausen, B. S.; Lengeler, B.; Topsoe, H. *Polyhedron* **1986**, *5*, 199.
(19) Caceres, C. V.; Fierro, J. L. G.; Blanco, M. N.; Thomas, H. J. *Appl. Catal.* **1984**, *10*, 333.
(20) Van Veen, J. A. R.; Gerkema, E.; Van der Kraan, A. M.; Hendricks, P. A. J. M.; Beens, H. *J. Catal.* **1992**, *133*, 112.
(21) Wivel, C.; Clausen, B. S.; Candia, R.; Morup, S.; Topsoe, H. *J. Catal.* **1984**, *87*, 497.
(22) Venezia, A. M.; LaParola, V.; Deganello, G.; Cauzzi, D.; Leonardi, G.; Predieri, C. *Appl. Catal., A* **2002**, *229*, 261.
(23) Okamoto, Y.; Ochiai, K.; Kawano, M.; Kobayashi, K.; Kubota, T. *Appl. Catal., A* **2002**, *226*, 115.
(24) Shimada, H. *Catal. Today* **2003**, *86*, 17.
(25) Ishihara, A.; Dumeignil, F.; Wang, D.; Li, X.; Arakawa, H.; Qian, E. W.; Inoue, S.; Muto, A.; Kabe, T. *Appl. Catal., A* **2005**, *292*, 50.
(26) Saih, Y.; Nagata, M.; Funamoto, T.; Masuyama, Y.; Segawa, K. *Appl. Catal., A* **2005**, *295* (1), 11.
(27) Rao, K. S. P.; Ramakrishna, H.; Murali Dhar, G. *J. Catal.* **1992**, *133*, 146.
(28) Maity, S. K.; Rana, M. S.; Srinivas, B. N.; Bej, S. K.; Murali Dhar, G.; Prasada Rao, T. S. R. *J. Molec. Catal. A* **2000**, *153*, 121.
(29) Damyanova, S.; Petrov, L.; Grange, P. *Appl. Catal., A* **2003**, *239*, 241.
(30) Bataille, F.; Lemberton, J. L.; Pérot, G.; Leyrit, P.; Cseri, T.; Marchal, N.; Kasztelan, S. *Appl. Catal., A* **2001**, *220*, 191.
(31) Murali Dhar, G.; Srinivas, B. N.; Rana, M. S.; Kumar, M.; Maity, S. K. *Catal. Today* **2003**, *86*, 45.
(32) Rana, M. S.; Maiti, S. K.; Ancheyta, J.; Murali Dhar, G.; Prasada Rao, T. S. R. *Appl. Catal., A* **2003**, *253*, 165.
(33) Rana, M.; Maity, S. K.; Ancheyta, J.; Murali Dhar, G.; Prasada Rao, T. S. R. *Appl. Catal., A* **2004**, *268*, 89.
(34) Damyanova, S.; Petrov, L.; Centeno, M. A.; Grange, P. *Appl. Catal., A* **2002**, *224*, 271.
(35) Grzechowiak, J. R.; Wereszczako-Zielinska, I.; Rynkowski, J.; Ziolek, M. *Appl. CataL. A* **2003**, *250*, 95.
(36) Dumeignil, F.; Sato, K.; Imamura, M.; Matsubayashi, N.; Payen, E.; Shimida, H. *Appl. Catal., A* **2006**, *315*, 18.
(37) Kresge, C. T.; Leonowicz, M. E.; Roth, W. J.; Vartuli, J. C.; Beck, J. S. *Nature* **1992**, *359*, 710.
(38) Beck, J. S.; Vartuli, J. C.; Roth, W. J.; Leonowicz, M. E.; Kresge, C. T.; Schmitt, K. D.; Chu, C. T. W.; Olson, D. H.; Sheppard, E. W.; McCullen, S. B.; Higgins, J. B.; Schlenker, J. L. *J. Am. Chem. Soc.* **1992**, *114*, 10834.
(39) Ciesla, U.; Schuth, F. *Microporous Mesoporous Mater.* **1999**, *27*, 131.
(40) Taguchi, A.; Schuth, F. *Microporous Mesoporous Mater.* **2005**, *77*, 1.
(41) Trong On, D.; Desplantier-Giscard, D.; Danumah, C.; Kaliaguine, S. *Appl. Catal., A* **2001**, *222*, 299.
(42) Schuth, F. *Chem. Mater.* **2001**, *13*, 3184.
(43) Yu, C.; Tian, B.; Zhao, D. *Curr. Opin. Solid State Mater. Sci.* **2003**, *7*, 191.
(44) Bagshaw, S. A.; Pinnavaia, T. J. *Angew. Chem., Int. Ed.* **1996**, *35*, 1102.
(45) Vaudry, F.; Khodabandeh, S.; Davis, M. E. *Chem. Mater.* **1996**, *8*, 1451.
(46) Valange, S.; Guth, J. -L.; Kolenda, F.; Lacombe, S.; Gabelica, Z. *Micro. Meso. Mater.* **2000**, *35−36*, 597.
(47) Antonelli, D. M.; Ying, J. Y. *Angew. Chem., Int. Ed.* **1995**, *34*, 2014.
(48) Antonelli, D. M.; Ying, J. Y. *Angew. Chem., Int. Ed.* **1996**, *35*, 426.
(49) Stone, V. F., Jr.; Davis, R. J. *Chem. Mater.* **1998**, *10*, 1468.
(50) Ciesla, U.; Schacht, S.; Stucky, G. D.; Unger, K. K.; Schuth, F. *Angew. Chem., Int. Ed.* **1996**, *35*, 541.
(51) Hudson, M. J.; Knowles, J. A. *J. Mater. Chem.* **1996**, *6*, 89.
(52) Wong, M. S.; Antonelli, D. M.; Ying, J. Y. *Nanostruct. Mater.* **1997**, *9*, 165.
(53) Wong, M. S.; Ying, J. Y. *Chem. Mater.* **1998**, *10*, 2067.
(54) Terribile, D.; Trovarelli, A.; de Leitenburg, C.; Dolcetti, G. *Chem. Mater.* **1997**, *9*, 2676.
(55) Sorensen, A. C.; Fuller, B. L.; Eklund, A. G.; Landry, C. C. *Chem. Mater.* **2004**, *16*, 2157.
(56) Sampieri, A.; Pronier, S.; Blanchard, J.; Breysse, M.; Brunet, S.; Fajerwerg, K.; Louis, C.; Perot, G. *Catal. Today* **2005**, *107−108*, 537.
(57) Muthu Kumaran, G.; Garg, S.; Soni, K.; Kumar, M.; Sharma, L. D.; Murali Dhar, G.; Rama Rao, K. S. *Appl. Catal., A* **2006**, *305*, 123.
(58) Reddy, K. M.; Wei, B.; Song, C. *Catal. Today* **1998**, *43*, 261.
(59) Chiranjeevi, T.; Kumar, P.; Rana, M. S.; Murali Dhar, G.; Prasada Rao, T. S. R. *J. Mol. Catal. A* **2002**, *181*, 109.
(60) Silva-Rodrigo, R.; Calderon-Salas, C.; Melo-Banda, J. A.; Dominguez, J. M.; Vazquez-Rodriguez, A. *Catal. Today* **2004**, *98*, 123.
(61) Zepeda, T. A.; Fierro, J. L. G.; Pawelec, B.; Nava, R.; Klimova, T.; Fuentes, G. A.; Halachev, T. *Chem. Mater.* **2005**, *17*, 4062.
(62) Zepeda, T. A.; Halachev, T.; Pawelec, B.; Nava, R.; Klimova, T.; Fuentes, G. A.; Fierro, J. L. G. *Catal. Commun.* **2006**, *7*, 33.
(63) Zepeda, T. A.; Pawelec, B.; Fierro, J. L. G.; Halachev, T. *J. Catal.* **2006**, *242*, 254.
(64) Gutierrez, O. Y.; Fuentes, G. A.; Salcedo, C.; Klimova, T. *Catal. Today* **2006**, *116*, 485.
(65) Cedeno, L.; Hernandez, D.; Klimova, T.; Ramirez, J. *Appl. Catal., A* **2003**, *241*, 39.
(66) Guttierez, O. Y.; Perez, F.; Fuentes, G. A.; Bokhimi, X.; Klimova, T. *Catal. Today* **2008**, *130*, 292.
(67) Hicks, R. W.; Castagnola, N. B.; Zhang, Z; Pinnavaia, T. J.; Marshall, C. L. *Appl. Catal., A* **2003**, *254*, 311.
(68) Kaluza, L.; Zdrazil, M.; Zilkova, N.; Cejka, J. *Catal. Commun.* **2002**, *3*, 151.
(69) Zhang, Z.; Pinnavaia, T. J. *J. Am. Chem. Soc.* **2002**, *124*, 12294.
(70) Hicks, R. W.; Pinnavaia, T. J. *Chem. Mater.* **2003**, *15*, 78.
(71) Kim, Y.; Kim, C.; Yi, J. *J. Non-Cryst. Solids* **2005**, *351*, 550.
(72) Lee, H. C.; Kim, H. J.; Rhee, C. H.; Lee, K. H.; Lee, J. S.; Chung, S. H. *Microporous Mesoporous Mater.* **2005**, *79*, 61.
(73) Niesz, K.; Yang, P.; Samorjai, G. A. *Chem. Commun.* **2005**, 1986.
(74) Royer, S.; Leroux, C.; Chaumonnot, A.; Revel, R.; Morin, S.; Rouleau, L. *Stud. Surf. Sci. Catal.* **2007**, *165*, 231.
(75) Boissière, C.; Nicole, L.; Gervais, C.; Babonneau, F.; Antonietti, M.; Amenitsch, H.; Sanchez, C.; Grosso, D. *Chem. Mater.* **2006**, *18*, 5238.
(76) Liu, Q.; Wang, A.; Wang, X.; Zhang, T. *Microporous Mesoporous Mater.* **2006**, *92*, 10.
(77) Liu, Q.; Wang, A.; Wang, X.; Gao, P.; Wang, X.; Zhang, T. *Microporous Mesoporous Mater.* **2007**, in press.
(78) May, M.; Navarrete, J.; Asomoza, M; Gomez, R. *J. Porous Mater.* **2007**, *14*, 159.

**Table 1. Main Parameters Used for the Synthesis of the Alumina Supports**

| sample name | Al precursor | templating agent | solvent | $T_{synthesis}$ (°C) | procedure | $T_{cal}$ (°C) |
|---|---|---|---|---|---|---|
| Al-Ref | Al-*sec*-butoxide | none | not known | | alkoxyde hydrolysis | 550 |
| Al-SolGel | Al-*sec*-butoxide | none | Butanol | 85 | Alkoxyde hydrolysis | 550 |
| $Al_{alk}$-S+ | Al-*sec*-butoxide | CTABr | butanol | 40 | alkoxyde hydrolysis | 550 |
| $Al_{nit}$-S0 | hydrated Al nitrate | P123 | $H_2O$ | 40 | salt neutralization | 600 |
| $Al_{alk}$-S0 | Al-*sec*-butoxide | P123 | butanol | 40 | alkoxyde hydrolysis | 550 |
| $Al_{alk\text{-}HCl}$-S0 | Al-*ter*-butoxide | P123 | ethanol (+ HCl) | 40 | alkoxyde hydrolysis | 550 |

thiophene, respectively. Nevertheless, complementary characterization seems necessary to conclude on the effect of the mesostructuration of the alumina support on the properties of the active phase. Further, recent developments in the synthesis methods for yielding mesostructured alumina enable the preparation of new samples with different morphologies and physical properties,[69−78] giving new opportunities for further catalytic developments.

In this work, a variety of mesoporous alumina samples were synthesized following procedures recently described in the literature. The obtained supports were characterized by X-ray diffraction (XRD), $N_2$ porosimetry and transmission electron microscopy (TEM). The CoMo catalysts prepared using these supports were fully characterized; TEM was used to obtain important information on the length and the stacking of the $MoS_2$ active phase. Catalytic performances of the samples were evaluated using the thiophene HDS model reaction. All the results were compared with those obtained for a commercial $\gamma$-$Al_2O_3$ and a laboratory-optimized sol−gel $Al_2O_3$ taken as references.

## 2. Experimental Section

**2.1. Supports Synthesis.** The synthesis of mesoporous alumina described in the literature is generally achieved by controlled hydrolysis of alkoxide precursors,[44,45,70,73,79] dissolved in an alcohol but in some cases precipitation of inorganic alumina precursors is preferred.[69,79] In the present work, a reference alumina was synthesized by a sol−gel method using a complexing agent for better control of the hydrolysis step. Three other samples were also synthesized by hydrolysis of an alkoxide precursor, one in the presence of a cationic surfactant and two in the presence of a nonionic templating agent. A last sample was prepared by nitrate salt precipitation in the presence of the same nonionic templating agent. The synthesis methods are detailed in the following paragraphs. The main synthesis parameters are gathered in Table 1. A commercially available $\gamma$-alumina support was also selected as a basis of comparison.

*2.1.1. Reference Commercial Alumina (Al-Ref).* The Al-Ref sample is a commercially available $\gamma$-$Al_2O_3$. Prior to use, surface of the solid was cleaned at 550 °C (temperature increase rate = 5 °C $min^{-1}$, isothermal time = 6 h) under air.

*2.1.2. Sol−gel Alumina (Al-SolGel).* The synthesis conditions of the Al-SolGel sample have been previously optimized to maximize the HDS catalytic activity, as described elsewhere.[9,80] The selected hydrolysis ratio ($H_2O$/aluminum tri*sec*-butoxide = 10) leads to a solid with a large pore volume and a high specific surface area (SSA).[80] In this procedure, aluminum tri-*sec*-butoxide (50 mL) was dissolved in 2-butanol (150 mL) under stirring at 85 °C. A complexing agent (35 mL of butan-1,3-diol) was added to the solution. Then, the aluminum alkoxide hydrolysis was performed by addition of water under vigorous stirring (35 mL of water). After being aged for 1 h at 85 °C under stirring, the solution was kept for one more hour under static conditions at room temperature. The powder obtained after evaporation under a primary vacuum at 40 °C was dried overnight at 100 °C before subsequent calcination at 550 °C under air for 6 h (temperature increase rate = 1 °C $min^{-1}$).

*2.1.3. Synthesis with Cationic Surfactant ($Al_{alk}$−S+).* The use of cationic directing agent for the synthesis of mesostructured alumina has been reported by others.[81−83] The synthesis procedure of $Al_{alk}$−S+ is essentially similar to this reported by Lee et al. using controlled hydrolysis of an aluminum alkoxide precursor in the presence of cetyl-trimethylammonium bromide (CTABr), except that ethanol is used as a solvent instead of 1-butanol, and calcination conditions slightly differ from those used by Lee et al. Unlike Al-SolGel, no complexing agent was used. Aluminum-tri-*sec*-butoxide (48.3 g) was initially dissolved in ethanol (EtOH; 45 g) placed under stirring at 40 °C. Then, the solution containing the surfactant (35.7 g of CTABr dissolved in 45 g of ethanol) was slowly added under vigorous stirring. After 1 h, water (7 mL) was added. The obtained compact vitreous gel (molar composition: 1 Al:0.5 CTABr:10 EtOH:2 $H_2O$) was aged 3 h at 40 °C before autoclaving for 20 h at 100 °C in the mother liquor. The solid was collected by filtration and dried at 110 °C overnight. Calcination was performed under the same conditions as for the Al-SolGel sample.

*2.1.4. Synthesis with Nonionic Surfactant $EO_{20}$-$PO_{70}$-$EO_{20}$ ('Pluronic P123').* Several references concerning the synthesis of mesoporous alumina using different nonionic directing agents can be found.[69,70,73,75,77,84−86] Fibrillar,[69,70] whormhole-like,[69,70] or hexagonal[73,75] morphologies are observed. We chose P123 as a nonionic surfactant as this copolymer is widely used for the synthesis of mesoporous silica. Moreover, it presents many advantages such as low cost, biodegrability, and ability to be used in a wide range of pH, temperature, and concentration in solution.

(a) Nitrate Precursor ($Al_{nit}$-S0). The synthesis procedure, which is similar to the synthesis of MSU-type $Al_2O_3$ solids, is inspired from the work of Zhang and Pinnavaia.[69] Nonahydrated aluminum nitrate (73.5 g) was dissolved in water (34 g) at 40 °C under stirring. After a clear solution was obtained, triblock copolymer (P123; 12.5 g) was added. The stirring was maintained for 36 h. The white precipitate (molar composition: 1 Al:0.017 P123:22 $H_2O$:2.6 $NH_4OH$) obtained by quick addition of concentrated $NH_4OH$ (until pH 8.5) was aged at ambient temperature for 48 h, filtered,

(79) Zhang, Z.; Hicks, R. W.; Pauly, T. R.; Pinnavaia, T. J. *J. Am. Chem. Soc.* **2002**, *124*, 1592.
(80) Dumeignil, F.; Sato, K.; Imamura, M.; Matsubayashi, N.; Payen, E.; Shimida, H. *Appl. Catal., A* **2003**, *241*, 319.
(81) Cabrera, S.; El Haskouri, J.; Alamo, J.; Beltran, A.; Beltran, D.; Mendioroz, S.; Dolores Marcos, M.; Amoros, P. *Adv. Mater.* **1999**, *11*, 379.
(82) Zhang, X.; Zhang, F.; Chan, K. -Y. *Mater. Lett.* **2004**, *58*, 2872.
(83) Aguado, J.; Escola, J. M.; Castro, M. C.; Paredes, B. *Appl. Catal., A* **2005**, *284*, 47.
(84) Zhang, Z.; Hicks, R. W.; Pauly, T. R.; Pinnavaia, T. J. *J. Am. Chem. Soc.* **2002**, *124* (8), 1592.
(85) Deng, W.; Bodart, P.; Pruski, M.; Shanks, B. H. *Microporous Mesoporous Mater.* **2002**, *52*, 169.
(86) Ruihong, Z.; Feng, G.; Yongqi, H.; Huanqi, Z. *Microporous Mesoporous Mater.* **2006**, *93*, 212.

**Table 2. Structural Properties of the Calcined Alumina Supports**

| sample name | $S_{BET}$ ($m^2\ g^{-1}$) | pore size[b]/ nm | pore volume[c] ($cm^3\ g^{-1}$) | water pore volume($cm^3\ g^{-1}$) | distribution type[d] | crystal phase[e] | morphology[f] |
|---|---|---|---|---|---|---|---|
| Al-Ref | 250[a] | 10.4 | 0.68 | 1.3 | L | $\gamma$ | Aggregates |
| Al-SolGel | 349 | 10.7 | 0.81 | 1.6 | F | $\gamma$ | Aggregates, fibrillar |
| $Al_{alk}$-S+ | 423 | 6.2 | 0.85 | 1.5 | F | $\gamma$ | Fibrillar |
| $Al_{nit}$-S0 | 358 | 5.3 | 0.60 | 1.1 | F | $\gamma$ | Fibrillar |
| $Al_{alk}$-S0 | 343 | 11.6 20.5 | 2.00 | 3.1 | L-bimodal | $\gamma$ | Fine fibrillar |
| $Al_{alk\text{-}HCl}$-S0 | 393 | 6.7 | 0.77 | 1.2 | F | Amorphous | 2D hexagonal |

[a] Maker specification. [b] Determined as shown in Figure 2 for Al-Ref (pore diameter taken at the middle of the segment defined by the width at half the height of the peak). [c] Evaluated for $P/P_0 > 0.995$. [d] F = fine, L = large. [e] Determined by comparison of the XRD patterns with the JCPDS files. [f] As observed by TEM.

washed with distilled water, and dried at 110 °C overnight. Calcination was performed at 600 °C for 6 h (temperature increase rate = 1 °C $min^{-1}$).

(b) Alkoxide Precursor ($Al_{alk}$-S0). The $Al_{alk}$-S0 sample was synthesized following the procedure described by Zhang et al.[87] P123 (23 g) was first dissolved in butanol (130 g) at 40 °C under stirring continuously maintained overnight. Then, aluminum-tri*sec*-butoxide (44.8 g) was slowly added to the solution. After 1/2 h of stirring, hydrolysis was performed by slow addition of a solution of water (10.6 g) and butanol (10 g). The obtained gel (molar composition: 1 Al:0.02 P123: 10.3 ButOH:3.2 $H_2O$) was then aged at 40 °C under static conditions for 30 h, filtered, washed with distilled water, and dried at 100 °C overnight. The solid was finally obtained by calcination at 550 °C under air for 6 h (temperature increase rate = 1 °C $min^{-1}$).

(c) Alkoxide Precursor in Acidified Medium ($Al_{alk\text{-}HCl}$-S0). The $Al_{alk\text{-}HCl}$-S0 sample was obtained following the procedure described by Niesz et al.[73] Similarly to the synthesis of SBA-15 type silica based materials, slow hydrolysis and condensation of the aluminum precursor occurs in the presence of the templating agent in acidified medium. A solution of 37 wt.% HCl (33.6 g) in EtOH (90 g) was slowly added under vigorous stirring to a solution of P123 structuring agent (19.3 g) previously dissolved in dried EtOH (181 g) at 40 °C. Aluminum-tri*tert*-butoxide (48.3 g) was then slowly added to this solution under vigorous stirring. The above parameters give a molar composition of 1 Al:0.017 P123:30 EtOH:6 $H_2O$:1.74 HCl. After half an hour, the stirring speed was slowed down, and the solvent was evaporated under dry $N_2$ flowing. After 4 days at 40 °C under dry $N_2$, the obtained viscous liquid was dried at 100 °C for 2 days. The white-yellowish powder was calcined at 550 °C under pure oxygen for 6 h (temperature increase rate = 1 °C $min^{-1}$).

**2.2. Catalyst Preparation.** After determination of the water pore volume of each carrier (Table 2), the catalysts were prepared by simultaneous incipient wetness impregnation of cobalt nitrate ($Co(NO_3)_3 \cdot 9H_2O$, Fluka 99%) and AHM ($(NH_4)_6Mo_7O_{24} \cdot 4H_2O$, Fluka 98%) as described elsewhere.[9,10] The formulation was adjusted to yield 10 wt % of molybdenum and a Co/(Co+Mo) ratio of 0.4 on the calcined oxide precursor. These values correspond to the limit on $Al_{nit}$-S0 that exhibits the lower water pore volume (Table 2; 1.1 $cm^3\ g^{-1}$), which is a decisive parameter that imposes the maximal quantity of active phase that can be loaded while achieving a good dispersion. After impregnation and maturation for 2 h, the obtained solids were dried overnight in an oven at 110 °C and calcined at 500 °C during 3 h with a temperature increase rate of 1 °C $min^{-1}$ under air flow.

For comparison purposes, all the catalysts were similarly activated by sulfidation under atmospheric pressure of the oxidic precursors during 2 h at 400 °C (temperature increase rate = 6 °C $min^{-1}$) under a flow of 10 vol % of $H_2S$ in $H_2$ (60 mL $min^{-1}$).

**2.3. Physical Characterization.** *2.3.1. Texture.* $N_2$ adsorption−desorption isotherms were recorded at −196 °C using an automated ASAP2010 instrument from MICROMERITICS. Before each run, a known mass of sample (around 0.200 g) was heated at 350 °C under vacuum for 3 h. SSAs were calculated from the linear part of the Brunauer−Emmett−Teller line.[88] Pore size distributions were obtained applying the Barrett−Joyner−Halenda (BJH) equation to the desorption branch of the isotherm.[88] Total pore volume was estimated from the $N_2$ uptake at a $P/P_0$ value of 0.995.

*2.3.2. Structure.* Powder X-ray diffraction patterns of the supports were collected on a SIEMENS D5000 diffractometer equipped with a Cu K$\alpha$ anticathode ($\lambda$ = 1.5406 Å). The diffractograms were recorded for $2\theta$ values comprised between 10 and 70° using a 0.1° step with an integration time of 4 s. Phase identification was carried out by comparison with the JCPDS database.

Transmission electronic microscopy (TEM) was used to determine the initial morphologies of the supports and the morphology of the supports after the impregnation/sulfidation procedure, as well as to evaluate the repartition in size and stacking of the $MoS_2$ slabs present on the sulfided catalysts. The TEM pictures were taken on a TECNAI electron microscope operating at an accelerating voltage of 200 kV. Before analysis, the powders were ultrasonically dispersed in ethanol. Two drops of ethanol containing the solid were then deposited on a carbon−copper grid.

To check the good dispersion of the molybdate phase, we recorded the Raman spectra of the oxidic precursors at room temperature using an Infinity Raman microprobe from Jobin-Yvon, equipped with a photodiode array detector. The exciting laser source was the 532 nm line of a Nd:YAG laser.

**2.4. Thiophene HDS Catalytic Test.** Thiophene was chosen as a model molecule to evaluate the catalytic performances of the catalysts, as usually found in the literature.[9,10,13−15,19−22]

The tests were performed at atmospheric pressure in a flow-type reactor packed with 0.2 g of catalyst. Before reaction, the oxidic precursor was sulfided as described in Experimental Section. The reactor was then naturally cooled to the reaction temperature of 300 °C under the sulfidation mixture. Thiophene, which was previously purified by two successive vacuum distillations, was introduced in the reactor at a constant pressure of 6.65 kPa in a flow of hydrogen (total flow rate = 10 mL $min^{-1}$). Reactants and products (butane, but-1-ene, trans-but-2-ene, cis-but-2-ene) were analyzed using a gas chromatograph equipped with a flame ionization detector and a Plot-alumina column. Taking into account the relative response factor for each compound, $\alpha$, the conversion, was calculated using the following equation:

(87) Zhang, W.; Pinnavaia, T. J. *Chem. Commun.* **1998**, 1185.

(88) Gregg, S. J.; Sing, K. S. W. *Adsorption, Surface Area and Porosity*; Academic Press: London, 1967.

$$\alpha = \frac{\sum_{i=1}^{4} \frac{a_i}{4}}{\frac{a_{\text{thio}}}{3.4} + \sum_{i=1}^{4} \frac{a_i}{4}}$$

where $a_i$ is the peak area corresponding to the $i$ product and $a_{\text{thio}}$ is the area of the peak of thiophene.

## 3. Results and Discussion

**3.1. Support Characterization.** The physical properties of the calcined alumina supports are summarized in Table 2 and partly in Table 3. Al-Ref presents the lowest SSA (250 $m^2\ g^{-1}$). Larger SSAs of about 350 $m^2.g^{-1}$ are observed for Al-SolGel, $Al_{nit}$-S0 and $Al_{alk}$-S0. The largest SSAs are obtained for $Al_{alk\text{-}HCl}$-S0 (393 $m^2\ g^{-1}$) and $Al_{alk}$-S+ (423 $m^2\ g^{-1}$). The $N_2$ adsorption desorption isotherms are presented in Figure 1. Except for $Al_{alk}$-S0, type IV isotherms with H2 type hystereses loop (IUPAC classification[88]) are observed, which is characteristic of mesoporous solids. Well-defined plateaus are observed on the $N_2$ adsorption−desorption isotherms at high $P/P_0$. They are characteristic of the $N_2$ capillary condensation into the mesopores. In contrast, $Al_{alk}$-S0 exhibits a type II isotherm, which indicates an open surface or a macroporous structure. In addition to this particularity, compared to the other samples, which exhibit a pore volume comprising between 0.60 and 0.85 $cm^3\ g^{-1}$, $Al_{alk}$-S0 presents a much larger pore volume of 2 $cm^3\ g^{-1}$ (Table 2).

The pore size distributions are presented in Figure 2. Mean pore diameters are reported in Table 2. All the distributions are monomodal except for $Al_{alk}$-S0, which shows a bimodal distribution with two ranges of pores, one with a mean pore diameter estimated at around 12 nm and the other one around 20 nm. A broad pore size distribution is observed for Al-Ref, with a mean pore diameter of 10.4 nm but the broadest distribution is observed for $Al_{alk}$-S0. In

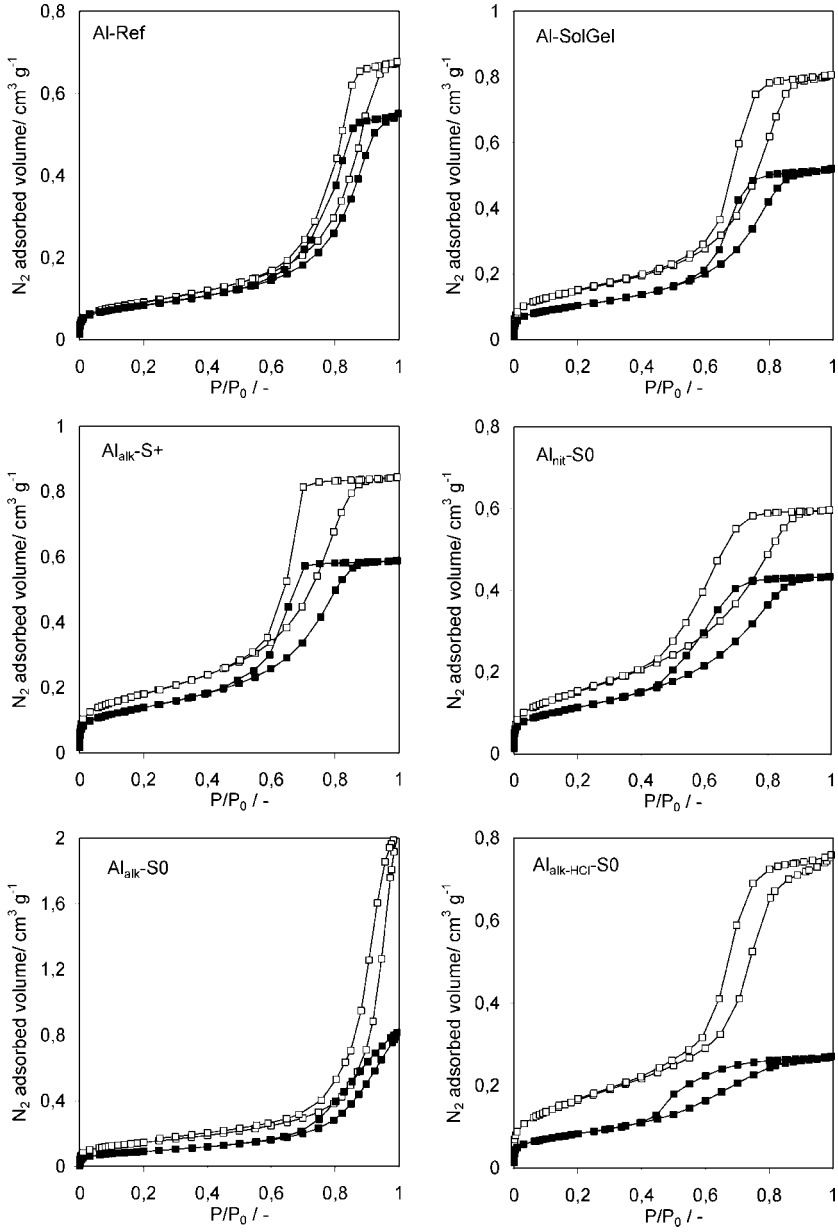


**Figure 1.** $N_2$ adsorption−desorption isotherms obtained on the calcined supports (open symbols) and the sulfided catalysts (full symbols).

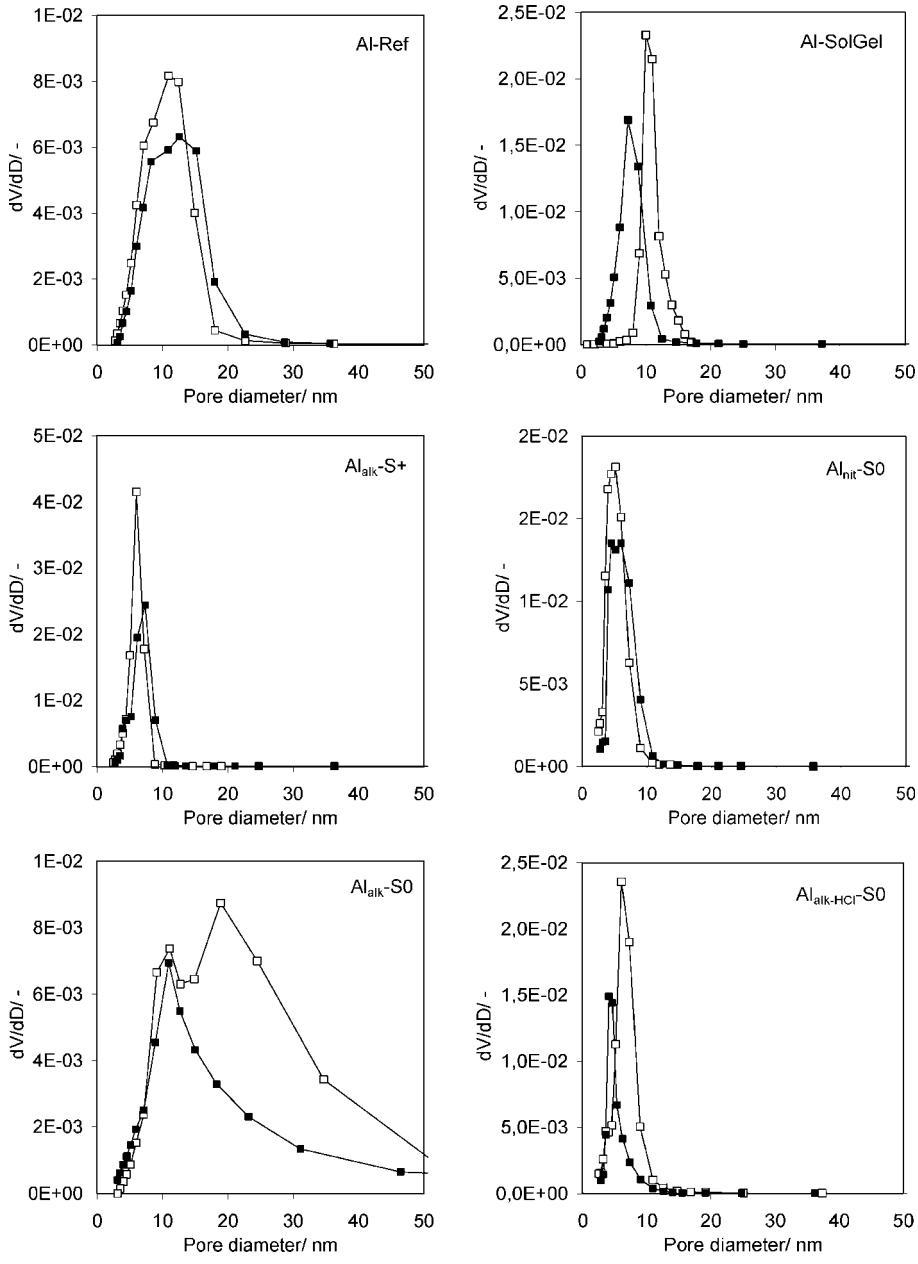


**Figure 2.** BJH pore size distribution obtained on the calcined supports (open symbols) and the sulfided catalysts (full symbols).

**Table 3. Physical Properties and Catalytic Activities of the Sulfided Catalysts**

| sample name | $S_{BET}$ ($m^2$ $g^{-1}$) (support) | $S_{BET}$ ($m^2$ $g^{-1}$) (catalyst) | $S_{BET}$ ($m^2$ $g^{-1}$) (catalyst after correction[a]) | SSA variation[b] (%) | mean pore diameter, $D_p$ (nm) (support) | mean pore diameter $D_p$ (nm) (catalyst) | $V_p$ ($cm^3$ $g^{-1}$) (support) | $V_p$ ($cm^3$ $g^{-1}$) (catalyst) | $V_p$ ($cm^3$ $g^{-1}$) (catalyst after correction[a]) | $V_p$ variation[b] (%) |
|---|---|---|---|---|---|---|---|---|---|---|
| Al-Ref | 250 | 196 | 254 | +2 | 10.4 | 11.5 | 0.68 | 0.55 | 0.71 | +4 |
| Al-SolGel | 349 | 243 | 315 | −10 | 10.7 | 7.8 | 0.81 | 0.52 | 0.67 | −17 |
| Al$_{alk}$-S+ | 423 | 324 | 421 | −0.5 | 6.2 | 7.0 | 0.85 | 0.6 | 0.78 | −8 |
| Al$_{nit}$-S0 | 358 | 266 | 345 | −3.5 | 5.3 | 6.2 | 0.60 | 0.44 | 0.57 | −5 |
| Al$_{alk}$-S0 | 343 | 215 | 279 | −19 | 11.6/20.5 | 13.4 | 2.00 | 0.81 | 1.05 | −47 |
| Al$_{alk-HCl}$-S0 | 393 | 196 | 254 | −35 | 6.7 | 4.5 | 0.77 | 0.27 | 0.35 | −54 |

[a] Correction is performed by removing the contribution of the weight gain consecutive to the introduction of the active phase (i.e., 23 wt % when considering the CoS and $MoS_2$ stoechiometries). [b] Relative to the value obtained on the bare support and the corrected value of the corresponding catalyst.

contrast, very sharp pore size distributions are obtained for Al$_{alk}$-S+, Al$_{nit}$-S0 and Al$_{alk-HCl}$-S0, the mean pore diameter varying between 5 and 7 nm. The observation of a sharp pore distribution is also characteristic of mesoporous solids. Almost similar pore size distribution is obtained for Al-SolGel, showing that the hydrolysis rate-controlled sol−gel method can give a solid with a fine pore distribution in the range of the mesopores. A slightly higher pore size (∼11 nm) is however obtained on this sample. Such sharp pore size distribution is not observed for Al$_{alk}$-S0, which exhibits again very different features (Figure 2). For this sample, the larger pore size explains the larger pore volume developed by this sample, compared to all the other mesostructured aluminas.

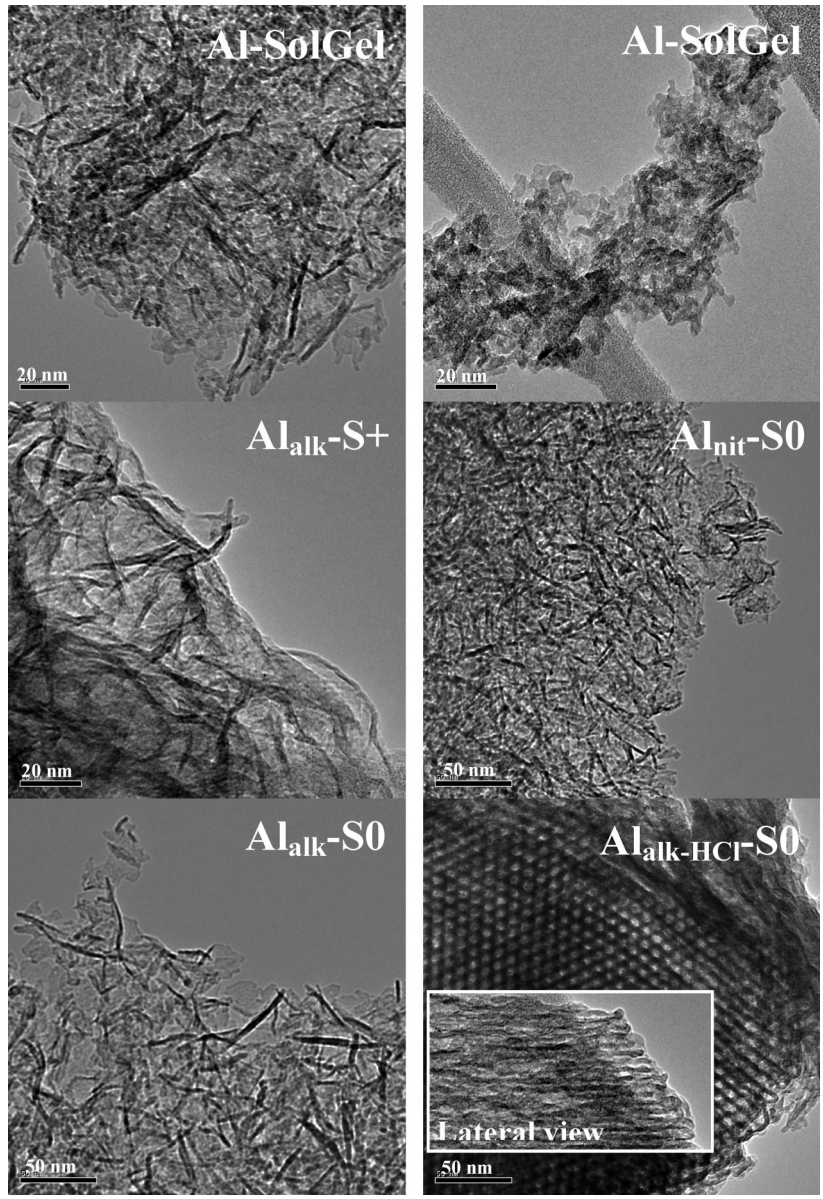


**Figure 3.** TEM pictures of the calcined supports.

The morphology of the different aluminas was observed by TEM. Representative pictures are shown in Figure 3. Except for $Al_{alk\text{-}HCl}$-S0, disordered structures are obtained: aggregates for Al-Ref (not shown), fibrillar structures for $Al_{alk}$-S+, $Al_{nit}$-S0, $Al_{alk}$-S0, and a mixed structure (aggregates + fibrillar) for Al-SolGel. The fibrillar morphology obtained by Zhang and Pinnavaia[69] on their MSU S/B samples is clearly observed for $Al_{nit}$-S0 (Figure 3). The morphology reported by Zhang and Pinnavaia[87] is also directly comparable to that obtained on the $Al_{alk}$-S0 sample. Fibrillar morphologies were also reported by Lee et al.[72] but from larger hydrolysis ratios ($R = [H_2O]/[Al]$ of 10 and 20) than that used in the present work ($R = 1$; $Al_{alk}$-S+). Using dry ethanol instead of 1-butanol as a solvent allowed us to obtain fibrillar morphologies at a much lower hydrolysis ratio. For this $Al_{alk}$-S+ sample, we obtained substantially higher pore volume and a fine pore size distribution (with still a type IV isotherm, Figure 1) keeping similar specific surface area, which makes this new modified procedure interesting for catalytic applications. $Al_{alk\text{-}HCl}$-S0 shows a very particular structure, the so-called ≪2D-hexagonal≫ structure, which is honeycomb-like, constituted of straight parallel pores with an hexagonal section, as already reported by Niesz et al.[73] When measured on the pictures, the thickness of the pore walls for this sample is around 2.5 nm and the pore diameter around 5.5 nm, to be compared with 6.7 nm obtained by $N_2$ adsorption. Note that less ordered structures could also be distinguished on some TEM pictures of this sample, which can explain this discrepancy.

The crystallographic structure of each sample was determined by XRD (Figure 4). Except for $Al_{alk\text{-}HCl}$-S0, which was completely amorphous, features corresponding to more or less crystallized $\gamma$-alumina (Table 2) were observed (main diffraction peak at $2\theta = 67°$). Note that in the case of $Al_{alk\text{-}HCl}$-S0, the organized pore network is maintained only if the alumina can keep its amorphous character. Indeed, Royer et al.[74] showed that crystallization of the walls and subsequent destruction of the 2D hexagonal structure were only observed after calcination at 1000 °C. On the basis of the peak intensity/sharpness, for the other supports the largest crystal-

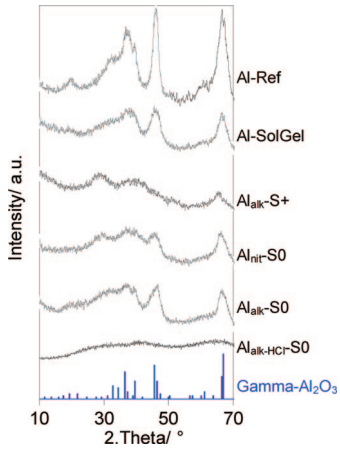


**Figure 4.** XRD diffractograms of the calcined supports. The diffractogram given for $\gamma$-alumina corresponds to JCPDS 16−0394.

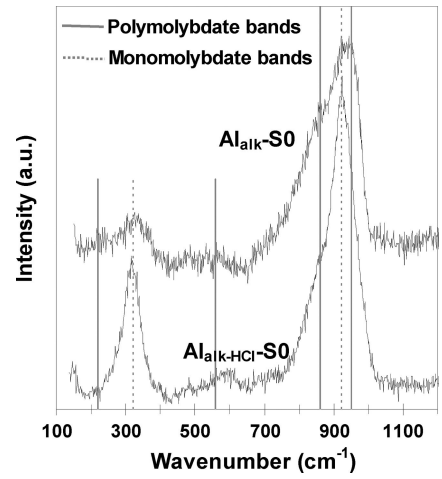


**Figure 5.** Typical Raman spectra of the oxidic precursors.

lization extent was obtained for Al-Ref, whereas the lowest was obtained for $Al_{alk}$-S+. This latter exhibited the largest specific surface area among all the synthesized solids.

It is interesting to note that compounds with similar physical properties can exhibit very different morphologies. This is the case of $Al_{alk\text{-}HCl}$-S0, which showed a SSA of 393 $m^2\ g^{-1}$ and a mean pore diameter of 6.7 nm, and $Al_{alk}$-S+, which shows a SSA of 423 $m^2\ g^{-1}$ and a mean pore diameter of 6.2 nm (Table 2). Although the former had a 2D-hexagonal structure, the latter exhibited a fibrillar morphology. In contrast, similar morphologies do not necessarily imply comparable physical properties. For example, $Al_{nit}$-S0 and $Al_{alk}$-S0 both showed fibrillar morphologies but their pore volumes (0.60 and 2.00 $cm^3\ g^{-1}$, respectively) as well as their mean pore diameter (5.3 nm monomodal and 11.6 nm/20.5 nm bimodal, respectively) were very different (Table 2). It appears then that a complete set of characterizations for each sample is mandatory to enable full knowledge of its physical and morphological properties.

Thus, an amorphous solid and more or less crystallized solids with high specific surface areas and large pore volumes were obtained. Alumina crystallization was accompanied with the formation of fibrillar structures (Figure 3). Only $Al_{alk\text{-}HCl}$-S0, which was found to be completely amorphous from a crystallographic point of view, exhibited an organized structure (hexagonal 2D structure), thus with amorphous walls.

**3.2. Catalyst Characterization.** *3.2.1. Characterization of the Oxidic Precursors.* Raman spectra were recorded to check the state of dispersion of the supported oxo-molybdate phase. No undesirable $MoO_3$ or $CoMoO_4$ phases were observed. This ensured that a good dispersion of the active phase precursor was achieved, irrespective of the sample. Thus, this parameter can be ruled out when comparing catalytic activities. However, the samples can be divided into two groups according to the type of oxo-molybdate species. For the first group constituted of $Al_{alk\text{-}HCl}$-S0 and $Al_{nit}$-S0, mainly monomolybdate species with characteristic lines[89] at 920 and 320 $cm^{-1}$ were observed, whereas for the second group constituted of Al-Ref, Al-SolGel, $Al_{alk}$-S+, and $Al_{alk}$-S0, polymolybdate species with characteristic lines[89] at 950, 860, 560, 360, and 220 $cm^{-1}$ were detected (examples in Figure 5). Monomolybdate entities were observed on the supports presenting the lowest pore volumes ($Al_{nit}$-S0 and $Al_{alk\text{-}HCl}$-S0) suggesting that physical properties such as the specific surface area or the pore size are not at the origin of the nature of the oxo-molybdate species. Thus, specific chemical surface properties could be responsible for the difference in oxo-molybdenum phase formation over mesostructured alumina.

*3.2.2. Characterization of Sulfided Solids.*

(a) Support Morphology. On the sulfided solids, i.e., on the activated catalysts, complete characterization was also performed. The properties of the sulfided samples are reported in Table 3.

No significant difference is observed on the TEM pictures between the supports (Figure 3) and the corresponding catalysts (Figure 6), except for $Al_{alk\text{-}HCl}$-S0. The hexagonal structure of this sample is not preserved upon the impregnation−calcination−sulfidation process. However, even if the hexagonal pore network is destroyed, a particular structure is still observed, with a kind of mosaic distribution of the pore mouths, as a footprint of the original 2D-hexagonal structure (Figure 6).

The SSA and pore volume of the catalysts must be corrected to enable direct comparison with the supports due to the contribution of the weight gain consecutive to the introduction of the active phase (i.e., 23 wt % when considering the CoS and $MoS_2$ stoechiometries). We can distinguish three groups of samples, corresponding to three behaviors. In the first group, represented by Al-Ref, $Al_{alk}$-S+ and $Al_{nit}$-S0, no significant variation of the intrinsic SSA and pore volume of the support was observed. This suggests that these samples are very stable and only slightly modified by the impregnation/sulfidation process. The second kind of behavior is observed for Al-SolGel with a slight decrease in both the SSA and the pore volume after catalyst preparation/activation. This sol−gel alumina seems then slightly less stable than the aforementioned samples, possibly due to the collapse of $\gamma$-$Al_2O_3$ crystallites during the impregnation and sulfidation process. For

(89) Payen, E.; Grimblot, J.; Lavalley, J.-C.; Daturi, M.; Maugé, F. *Handbook of Vibrational Spectroscopy*; Wiley & Sons: New York, 2001; Vol. 4, p 3005.

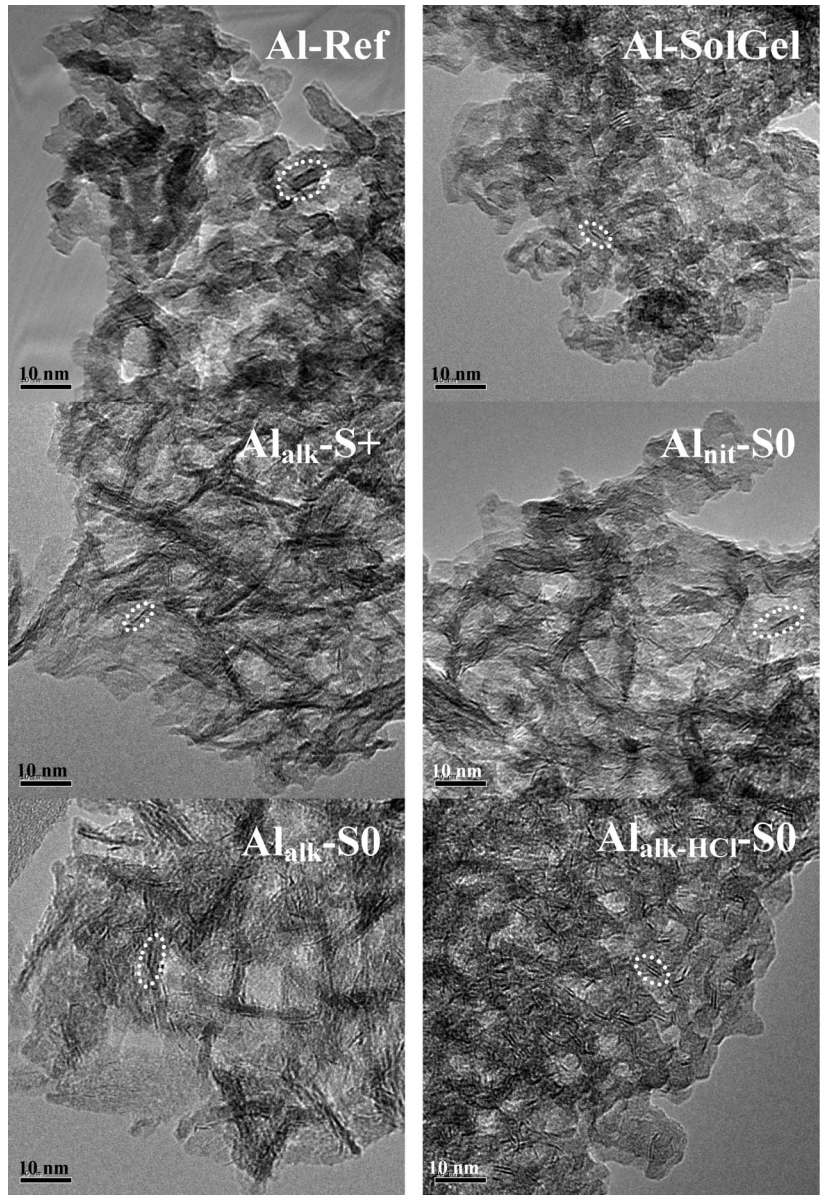


**Figure 6.** TEM images of the sulfided catalysts (the dashed ellipses indicate examples of slabs).

these two first groups of materials, the isotherm shape remains almost unchanged after the impregnation/sulfidation sequence, and only a slight decrease in pore volume and SSA is observed. This suggests a good distribution of the active metals through the pores network. In the third group containing $Al_{alk}$-S0 and $Al_{alk\text{-}HCl}$-S0, significant decreases in the surface area (respectively 19 and 35%) and in the pore volume (47 and 54%) are observed. The decrease in SSA observed for $Al_{alk\text{-}HCl}$-S0 might be linked with the structural modifications observed by TEM. A collapse of $\gamma$-$Al_2O_3$ crystallites during the impregnation/sulfidation process can explain this result but such drastic modifications might also originate in the segregation of a part of the active phase to the periphery of the alumina crystallite aggregates. But we note the presence of small $MoS_2$ slabs (average length of 1.89 nm; Table 4) sizes, as well as the absence of bulk Mo oxides as deduced from LRS results (Figure 5), suggesting a good distribution of the active phase on the whole available surface. In any case, the observed surface areas (larger than 200 $m^2$/g) and pore volumes of the catalysts (larger than ~0.6 $cm^3$/g) remain relatively important and compatible with further catalytic use.

**Table 4. Average Length and Average Stacking of the $MoS_2$ Slabs in the Sulfided Catalysts**

| sample name | average length (nm) | average stacking |
|---|---|---|
| Al-Ref | 2.07 | 1.11 |
| Al-SolGel | 2.27 | 1.18 |
| $Al_{alk}$-S+ | 1.85 | 1.17 |
| $Al_{nit}$-S0 | 1.91 | 1.16 |
| $Al_{alk}$-S0 | 1.89 | 1.07 |
| $Al_{alk\text{-}HCl}$-S0 | 1.76 | 1.33 |

Except for $Al_{alk}$-S0, no significant change in the pore size distribution was observed between the supports and the corresponding catalysts. For $Al_{alk}$-S+, $Al_{nit}$-S0 and $Al_{alk\text{-}HCl}$-S0, the distribution remained sharp with a mean pore diameter in the same range as before impregnation. An important change was however observed for the $Al_{alk}$-S0 solid, where only the smallest pores (~13 nm) remain on the catalyst. It seems that the steps of impregnation,

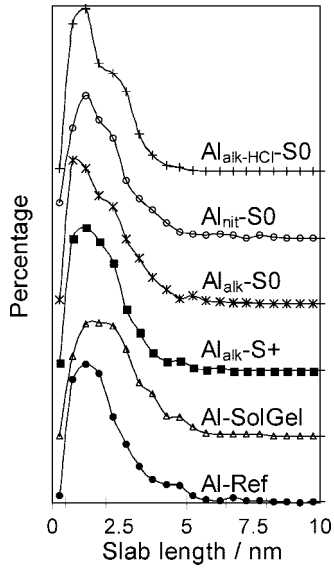


**Figure 7.** Distribution of $MoS_2$ slab lengths.

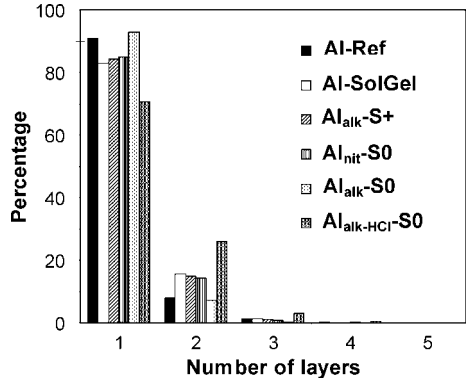


**Figure 8.** Stacking degree of $MoS_2$ slabs.

calcination, and sulfidation lead to the vanishing of the larger pores (~20 nm).

(b) Active Phase Morphology. TEM studies of the catalysts revealed the presence of structures typical of the layered $MoS_2$ phase, with a spacing of about 0.6 nm between the lattice fringes (Figure 6). Irrespective of the catalyst, the presence of large $MoS_2$ nodules was not observed, which shows that the good dispersion of the molybdenum observed at the oxidic state is still preserved at the sulfided state.[90] Note that although microscopy does not provide any direct evidence of the location of the $MoS_2$ slabs, there is a strong presomption of a good dispersion within the mesopore network. Indeed, LRS (Figure 5) showed that no $MoO_3$ or $CoMoO_4$ bulk species were formed and the outer surface of the particles would be insufficient to yield the good dispersion of the $MoS_2$ slabs that we actually evidenced.

Statistics were performed on ca. 1000 slabs comprising one or more layers. This enables reliable determination of the distribution of size and stacking for each sample (Figures 7 and 8). The average length of the slabs as well as the average number of layers in the slabs are presented in Table 4. These parameters play an important role on the HDS performances. It is now well admitted that the active sites are located on the edges of the $MoS_2$ slabs. The average slab length is correlated with the number of active sites (thus located at their periphery), and then with the HDS catalytic activity.[91] Consequently, a decrease in average slab length induces an increase in catalytic activity. Further, it has been claimed that selectivity can be tuned by modifying the stacking of the slabs.[92] However, the influence of this parameter might be more pronounced for S-containing aromatic molecules larger than thiophene, i.e., dibenzothiophene and substituted dibenzothiophenes.

The distribution of $MoS_2$ slabs lengths on each sample is shown in Figure 7. The samples prepared using P123 show a bimodal-like distribution, especially evident for Al$_{alk-HCl}$-S0. The other samples show a monomodal distribution, with a large profile for Al-SolGel. The samples prepared with a templating agent exhibit an average slab length (ASL) lower than *ca.* 1.9 nm (Table 4). In contrast, the ASL of Al-Ref and Al-SolGel were 2.1 and 2.3 nm, respectively. Among the templating agent-prepared catalysts, Al$_{alk-HCl}$-S0 had a significantly lower average slab length of 1.8 nm.

The $MoS_2$ slabs stacking distribution on each sample is shown in Figure 8. On Al-Ref and Al$_{alk}$-S0, more than 90% of the $MoS_2$ slabs are monolayered. Al-SolGel, Al$_{alk}$-S+ and Al$_{nit}$-S0 show equivalent distribution with *ca.* 84% of monolayered slabs and ca. 15% of bilayered slabs. Al$_{alk}$-HCl-S0 is distinguished by a lower percentage of monolayered slabs (ca. 71%), to the benefit of bilayered slabs (ca. 26%) with even more a slightly larger percentage of trilayered slabs of ca. 3% compared to that observed on all the other samples (around 1% or less). Accordingly, the average stacking values in Table 4 reflect the presence of three groups. Al-Ref and Al$_{alk}$-S0 gives a value of ca. 1.09, Al-SolGel, Al$_{alk}$-S+ and Al$_{nit}$-S0 gives a value of ca. 1.17 while Al$_{alk-HCl}$-S0 shows a significantly higher average stacking of 1.33. When visually comparing the TEM pictures (Figure 6), this specific multilayer-oriented structure can be distinguished at a glance.

These results point out the specificity of Al$_{alk-HCl}$-S0 sample among all the prepared catalysts. This sample exhibits a large stacking together with smaller slabs. This is indicative of the atypical behavior of this solid when used as a catalyst support as already presumed when considering its particular structure.

**3.3. Catalytic Activity.** The samples prepared in this work were tested in the thiophene HDS reaction after subsequent sulfidation. As previously mentioned, the thiophene is the simplest molecule representative of the aromatic sulfur compounds present in the feeds to be treated. Consequently, this test is commonly admitted as a reference HDS catalytic test.[13−15,19−22]

The thiophene HDS conversion of all the catalysts is reported in Table 5. Although the composition of the catalysts is identical, significantly different catalytic activities were observed. The lowest conversions were found for Al$_{alk-HCl}$-S0 (13%) and Al$_{nit}$-S0 (18%). Al-Ref (29%), Al-SolGel (31%), and Al$_{alk}$-S+ (32%) exhibited good performances.

(90) Payen, E.; Hubaut, R.; Kasztelan, S.; Poulet, O.; Grimblot, J. *J. Catal.* **1994**, *147*, 123.

(91) Kasztelan, S.; Toulhoat, H.; Grimblot, J.; Bonnelle, J.-P. *Appl. Catal.* **1984**, *13*, 127.

(92) Daage, M.; Chianelli, R. E. *J. Catal.* **1994**, *149*, 414.

**Table 5. Thiophene HDS Conversion of the Catalysts**

| sample name | conversion α (%) |
|---|---|
| Al-Ref | 29 |
| Al-SolGel | 31 |
| $Al_{alk}$-S+ | 32 |
| $Al_{nit}$-S0 | 18 |
| $Al_{alk}$-S0 | 38 |
| $Al_{alk\text{-}HCl}$-S0 | 13 |

The highest conversion was found over $Al_{alk}$-S0 (38%). Most of the physicochemical properties (SSA, pore size, etc., Table 3) vary according to the synthesis procedure. Nevertheless, no correlation between these physical properties and the catalytic activity can be evidenced. Moreover, Raman spectroscopy showed that the oxidic active phase is well-dispersed regardless of the support and thus activity differences cannot be related to the presence of some non-sulfidable species such as bulk $MoO_3$ or $CoMoO_4$. Similarly, the differences in morphology of the active phase (difference in slab size and stacking) as determined by TEM cannot explain the differences in thiophene conversion. Indeed, the less active solid ($Al_{alk\text{-}HCl}$-S0) exhibits the lowest $MoS_2$ slabs length as well as the highest stacking, which should confer good performances as previously proposed.[93−95]

However, Raman analysis showed that the nature of the oxo-species on the oxidic precursors depends on the support used. Although the presence of monomolybdate species was clearly identified over $Al_{alk\text{-}HCl}$-S0 and $Al_{nit}$-S0, all the other samples showed Raman features characteristic of the polymolybdate phase. The presence of monomolybdate species may be in some extent at the origin of the low activities of the corresponding catalysts. Indeed, it is well-known that monomolybdate entities are not well sulfidable.[96] This can be explained considering that the transformation of the oxomolybdate species into the $MoS_2$ phase implies O−S exchanges as well as successive reductions of the Mo atoms.[97] Because of the very low reducibility of the isolated monomolybdate entities, as shown by Hamraoui et al. using DFT calculations,[98] we may suggest that these monomeric entities evolve differently during the activation step, compared to the polymolybdate phase, thus leading to a "non-well-sulfided" phase. Consequently, the amount of $MoS_2$ nanocrystallites on the catalysts in which monomeric entities have been detected as major species should be lower than that on the catalysts containing polymolybdates. This further yields the presence of a lower number of sites that can accept Co as a promoter atom. At this point, we must also mention that, in this preliminary study, we did not check about the actual promotion effect of Co, which might be an important parameter. Indeed, the used Co/(Co+Mo) ratio is the classical one determined for conventional alumina supports considering that a large fraction of Co atoms (about 50 atomic %) are not sulfided because of the formation during the impregnation−drying−calcination sequence of a pseudo $CoAl_2O_4$ phase, which is not sulfidable. In the present work, we used new alumina supports that can have more or less affinity for the cobalt atoms. This should have an effect on the total amount of cobalt atoms that are in decoration position of the disulfide slabs. This point will be further investigated using series of catalysts with various atomic ratios Co/(Co+Mo).

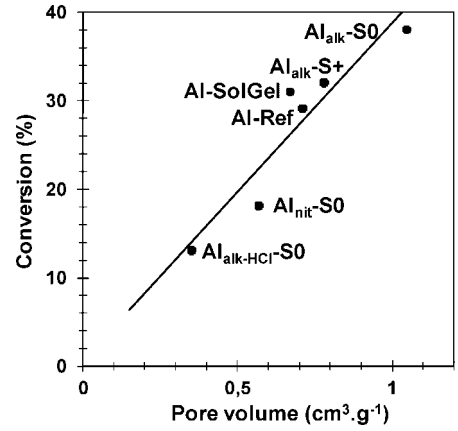


**Figure 9.** Correlation between the pore volume of the catalysts and their thiophene HDS conversion.

Moreover, a correlation between the pore volume and the conversion is observed (Figure 9). In a first approach, we classified the samples into two groups, the first one with monomolybdate species on lower pore volume supports (with lower activities) and the second one with polymolybdate species on larger pore volume supports (with larger activities). While clearly enlightening a boundary between the behaviors of these two groups, Figure 9 further suggests that a finer correlation exists within each group, with a manifest dependency of the conversion with the pore volume. However, with the available elements at this point, we cannot reliably interpret such an observation. But a very interesting point is that the most active solid was prepared using the alumina support ($Al_{alk}$-S0), which exhibited a fine fibrillar morphology and the largest water pore volume (i.e., 3.1 $cm^3\ g^{-1}$). As it has been shown for Mo-based catalysts, the Mo dispersion, i.e., the absence of $MoO_3$ or $CoMoO_4$ entities, is mainly governed by the pore volume of the support.[99] Thus, we can suppose that the $Al_{alk}$-S0 alumina might enable the preparation of HDS catalysts with well-dispersed active phases at higher amounts of supported Mo and Co species and consequently exhibiting higher activities.

## 4. Conclusions

The aim of this work was to evaluate the potential of mesoporous alumina solids as catalyst supports. A series of mesoporous aluminas was prepared using procedures recently described in the literature. The prepared powders were subsequently used as supports for CoMoS HDS catalysts, which were compared in terms of catalytic activity with two

(93) Sun, M.; Nicosa, D.; Prins, R. *Catal. Today* **2003**, *86*, 173.
(94) van Veen, J. A. R.; Gerkema, E.; van der Kraan, A. M.; Knoester, A. *J. Chem. Soc., Chem. Commun.* **1987**, 1684.
(95) Frizi, N.; Blanchard, P; Payen, E.; Baranek, P.; Lancelot, C.; Rebeilleau, M.; Dupuy, C.; Dath, J.-P. *Catal. Today* **2008**, *130*, 32–40.
(96) Grimblot, J.; Dufresne, P.; Gengembre, L.; Bonnelle, J. P. *Bull. Soc. Chim. Belge* **1980**, *20* (12), 1261.
(97) Weber, T.; Muijsers, J. C.; van Wolput, J.H.M.C.; Verhagen, C. P. J.; Niemantsverdriet, J. W. *J. Phys. Chem.* **1996**, *100*, 14144.
(98) Hamraoui, K.; Ph.D. Thesis Ministére de l' Enseignement Supérieur et de la Recherche, Lille, France, 2007.
(99) Lamonier, C.; Blanchard, P.; Guillaume, D.; Payen, E. *Stud. Surf. Sci.* **2006**, *162*, 713.

reference catalysts prepared from a commercial $\gamma$-$Al_2O_3$ and an optimized sol−gel alumina.

The mesoporous synthesis procedures used in this work were selected to obtain a set of different morphologies and physical properties. Thus, different aluminum sources and templating agent (cationic or nonionic) were used. Large specific surface areas were obtained for the mesoporous supports, with SSA exceeding 400 $m^2$ $g^{-1}$ when using a cationic surfactant. Mesostructured supports mainly exhibited a well-defined fibrillar morphology. Only one support showed a 2D hexagonal pore structure. Nevertheless, this sample was the only one that remained amorphous, from a crystallographic point of view, after calcination. All the other samples were constituted of a more or less crystallized $\gamma$-$Al_2O_3$ phase.

Different behaviors were observed concerning the physical and textural properties evolution during the impregnation-calcination-sulfidation cycle for yielding the final supported CoMoS active phase. Some solids underwent drastic textural changes. The best example is the support presenting a 2D hexagonal pore organization, for which the active phase preparation procedure resulted in some disruption of this hexagonal organization and in drastic decreases in both SSA and pore volume.

Slightly higher catalytic activities for the thiophene HDS were obtained using high surface area and high pore volume supports. The catalytic activity did not vary in parallel with the morphological parameters of the active phase. Finally, the catalysts could be divided into two groups. The first one including low conversion solids presented monomolybdate species before sulfidation. These monomolybdate entities, the formation of which being assigned to the surface chemical properties of these new carriers, are supposed to be responsible for the low activities of the corresponding catalysts. The second one, including high conversion solids, presented only polymolybdate species before sulfidation. Their activities seem to be correlated with the pore volume developed by the corresponding supports.

The most active solid was prepared using the alumina support ($Al_{alk}$-S0), which exhibited a fine fibrillar morphology and the largest water pore volume (i.e., 3.1 $cm^3$ $g^{-1}$). Moreover, as the limit for the achievement of a good Mo dispersion is mainly governed by the pore volume of the support, some of the prepared new supports especially constitute an interesting way for the preparation of very active HDS catalysts with larger metal loadings.

Thus, the mesostructured aluminas prove their potential in the simple thiophene HDS test; as a next step, we plan to specifically optimize the most promising ones for 4,6-DMDBT HDS.

**Acknowledgment.** The authors thank the European Union for financing a part of this research through the Contract MIRG-CT-2007-046383. The authors thank Mr. Gérard Cambien of the ECL, USTL, Villeneuve d'Ascq, who kindly recorded the $N_2$ adsorption−desorption isotherms of our solids.

CM802084E